

Missouri S&T

Missouri University of Science & Technology
Curtis Laws Wilson Library

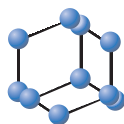
ILLIAD Electronic Delivery Cover Sheet

WARNING CONCERNING COPYRIGHT RESTRICTIONS

The copyright law of the United States (Title 17, United States Code) governs the making of photocopies or other reproductions of copyrighted materials. Under certain conditions specified in the law, libraries and archives are authorized to furnish a photocopy or other reproduction. One of these specified conditions is that the photocopy or reproduction is not to be "*used for any purpose other than private study scholarship, or research.*" If a user makes a request for, or later uses, a photocopy or reproduction for purposes in excess of "fair use," that user may be liable for copyright infringement.

This institution reserves the right to refuse to accept a copying order if, in its judgment, fulfillment of the order would involve violation of copyright law.

RESEARCH ARTICLE


**BENTHAM
SCIENCE**

The Primary Mechanism of Cellular Internalization for a Short Cell-Penetrating Peptide as a Nano-Scale Delivery System



Betty R. Liu^{1,*}, Yue-Wern Huang², Mallikarjuna Korivi³, Shih-Yen Lo¹, Robert S. Aronstam⁴ and Han-Jung Lee⁵

¹Department of Laboratory Medicine and Biotechnology, College of Medicine, Tzu Chi University, Hualien 97004, Taiwan; ²Department of Biological Sciences, Missouri University of Science and Technology, Rolla, MO 65409-1120, USA; ³College of Physical Education and Health Sciences, Zhejiang Normal University, Jinhua, Zhejiang, China; ⁴College of Science and Technology, Bloomsburg University of Pennsylvania, Bloomsburg, PA17815-1301, USA; ⁵Department of Natural Resources and Environmental Studies, National Dong Hwa University, Hualien 97401, Taiwan

Abstract: Background: Development of effective drug delivery systems (DDS) is a critical issue in health care and medicine. Advances in molecular biology and nanotechnology have allowed the introduction of nanomaterial-based drug delivery systems. Cell-penetrating peptides (CPPs) can form the basis of drug delivery systems by virtue of their ability to support the transport of cargoes into the cell. Potential cargoes include proteins, DNA, RNA, liposomes, and nanomaterials. These cargoes generally retain their bioactivities upon entering cells.

Method: In the present study, the smallest, fully-active lactoferricin-derived CPP, L5a is used to demonstrate the primary contributor of cellular internalization.

Results: The secondary helical structure of L5a encompasses symmetrical positive charges around the periphery. The contributions of cell-specificity, peptide length, concentration, zeta potential, particle size, and spatial structure of the peptides were examined, but only zeta potential and spatial structure affected protein transduction efficiency. FITC-labeled L5a appeared to enter cells via direct membrane translocation insofar as endocytic modulators did not block FITC-L5a entry. This is the same mechanism of protein transduction active in Cy5 labeled DNA delivery mediated by FITC-L5a. A significant reduction of transduction efficiency was observed with structurally incomplete FITC-L5a formed by tryptic destruction, in which case the mechanism of internalization switched to a classical energy-dependent endocytosis pathway.

Conclusion: These results support the continued development of the non-cytotoxic L5a as an efficient tool for drug delivery.

Keywords: Cell-penetrating peptides (CPPs), cellular internalization, direct membrane translocation, drug delivery system (DDS), lactoferricin, helical wheel projection, protein transduction domains (PTDs).

1. INTRODUCTION

Drug delivery systems are a major consideration in drug development. Efficient and biocompatible drug delivery systems can minimize side effects from drugs and increase drug safety. Therapeutic efficiency can be increased by increasing the absorption rate, reducing drug degradation and targeting drug release [1]. Drug delivery systems are no longer confined to the traditional oral delivery, injection, mucosal absorption,

or transdermal pathways [2]. Molecular biology, genetic medicine and nanotechnology have introduced novel modes of drug delivery [2]. Moreover, new materials and methods for drug targeting allow the use of nanomaterials, nucleic acids (plasmid DNA, siRNA, mRNA, and aptamer) and peptidic biochemicals (small peptide and protein) as therapeutic agents [3]. Investigations of drug delivery have focused on the development of novel delivery vehicles, identification of the routes of delivery, utilization of different types of cargoes, and refinement of targeting and release strategies [4]. In particular, the maturation of nanotechnology and the exploitation of nanomaterials have led to advances in drug delivery systems and the controlled release of therapeutic

*Address correspondence to this author at the Department of Laboratory Medicine and Biotechnology, College of Medicine, Tzu Chi University, Hualien 97004, Taiwan; Tel: +886-3-8565301 Ext. 2326; Fax: +886-3-8571917; E-mail: brliu7447@mail.tcu.edu.tw

molecules [1]. Nanoparticles can be manipulated with respect to size, shape and chemical functionality to broaden their applicability in drug delivery systems [3]. Many nanomaterials, such as micelles [4], liposomes [3], inorganic materials (e.g. gold nanoparticles, ferrofluids, quantum dots (QDs), and silica) [5, 6], and peptides [7], have been developed as drug or gene carriers and for use in diagnosis, and imaging. Nanomaterials derived from natural products often have additional advantages of safety and biodegradability.

Cell-penetrating peptides (CPPs) or protein transduction domains (PTDs) that are able to traverse cell membranes, thereby delivering various cargoes into living cells, have been introduced as novel harmless delivery vehicles [8, 9]. The first CPPs were derived from human immunodeficiency virus type 1 (HIV-1) transactivation of transcription (Tat) protein, which contains eleven basic-rich residues [10]. CPPs include amphipathic, hydrophobic and cationic peptides [11]. CPPs can be classified as naturally-derived, designed, and chimeric, depending on their source [12]. A CPP database has been published [13]. The ability of CPPs to deliver biologically active molecules, including proteins, nucleic acids, peptide nucleic acids, cytotoxic therapeutic drugs, inorganic particles and liposomes into cells has been widely reported [9, 12, 14]. CPPs form complexes with cargoes by different methods [15-19]. The cargoes that CPPs can deliver vary in size up to 200 nm in diameter [20]. CPPs are generally non-toxic to cells, tissues, and small organisms [21-27]. Therefore, CPPs are potent tools for delivering the therapeutic molecules in preclinical and clinical studies.

The antimicrobial peptide lactoferricin, derived from a glycoprotein rich in milk, saliva, tears, and mucous secretions in mammals, was recently identified as a CPP [28-30]. Many lactoferricin derivatives possess antiviral, antifungal, antimicrobial, antitumor, antiprotozoal, anticancer, and antihypertensive properties [31]. The antibacterial active domain of lactoferricin is located in its N-terminal region. The antimicrobial core region lactoferricin was found to be restricted to only six amino acids (RRWQWR) [31]. This core domain, termed bLFcin₆, possessed bactericidal potency as well as the ability to deliver small interfering RNA (siRNA) [32]. High transduction efficiency was observed with bLFcin₆ in HeLa cells, with no evidence of immunogenicity or cytotoxicity [32]. Cellular penetrating ability was observed with two lactoferricin derivatives: L5a (RRWQW) and L5b (RWQWR) [32, 33]. L5a delivered plasmid DNA into mammalian cells with a higher efficiency than L5b [33].

The mechanism underlying CPPs entry into cells is still controversial. Considerable evidence indicates that classical endocytosis-dependent pathway and direct membrane translocation are the major routes for CPPs uptake [34]. Many factors, including the types of CPPs and the nature of the cargo, appear to affect the internalization route [18, 35, 36]. The shortest CPP, L5a, displays high transduction efficiency at a low concentration and enters cells rapidly [33]. However, the mechanism of cellular internalization for L5a is still uncertain. In this study, we examined different factors that influence L5a internalization, and also analyzed the role of secondary structure of FITC-labeled L5a on internalization efficiency. Finally, we evaluated the possible mechanism for FITC-L5a internalization using various endocytosis modulators. The entry pathway for FITC-L5a with intact secondary

structures was compared to that of trypsin-treated FITC-L5a with altered structure.

2. METHODS AND MATERIALS

2.1. Cell Culture

Human bronchoalveolar carcinoma A549 cells (American Type Culture Collection, Manassas, VA, USA; CCL-185) were maintained in Roswell Park Memorial Institute (RPMI) 1640 medium (Gibco, Invitrogen, Carlsbad, CA, USA) supplemented with 10% (v/v) bovine serum (Gibco) [36]. Human embryonic kidney 293FT cells (HEK293FT, kindly provided from Dr. Chen, Hwei-Hsien, National Health Research Institutes, Taiwan), were maintained in Dulbecco's modified Eagle medium (DMEM) (Gibco) supplemented with 10% (v/v) fetal bovine serum (Gibco) [37, 38]. Living cells were determined using trypan blue stain. Cells were washed with phosphate buffered saline (PBS) three times before and after each treatment. The culture medium was switched to serum-free RPMI medium during each experiment.

2.2. Peptides and Plasmid DNA Preparation

Various fluorescein isothiocyanate (FITC) N-labeled peptides, including histidine-rich nona-arginine denoted as FITC-HR9 (CHHHHHRRRRRRRRHHHHHC) [35], 13-residues containing FITC-lactoferricin (CRRWQWRMKK-LGC) [28], FITC-L12 (FKCRRWQWRMKK), FITC-L11 (KCRRWQWRMKK), FITC-L9 (RRWQWRMKK), FITC-L6 (RRWQWR), FITC-L5a (RRWQW), and FITC-L5b (RWQWR) were chemically synthesized (Genomics, Taipei, Taiwan). Partial CPPs, such as FITC-L5a and FITC-L5b, were purchased from GMbiolab Co. Ltd. (Taichung, Taiwan). All peptides were purified and quantified by HPLC. The purities of products were $\geq 85\%$. The chemical structures and masses of all peptides used in experiments are shown in Table 1.

In experiments correlating peptide secondary-structures with cellular uptake, FITC-L5a was incubated with 0.4 μg of trypsin (Gibco) at 37°C for 1 h at an enzyme/substrate ratio of 1/100 [39].

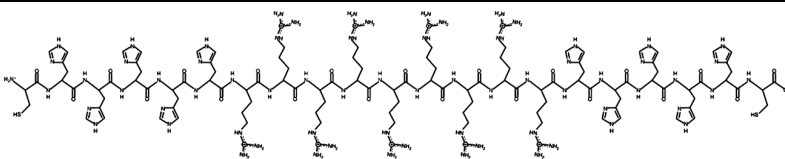
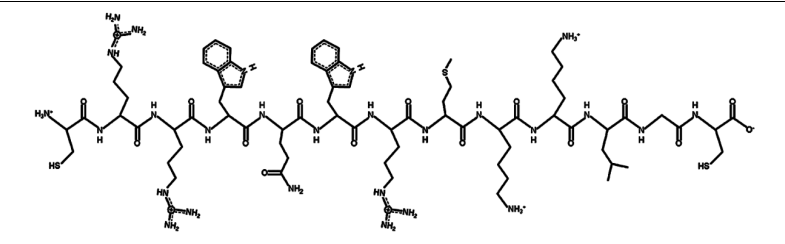
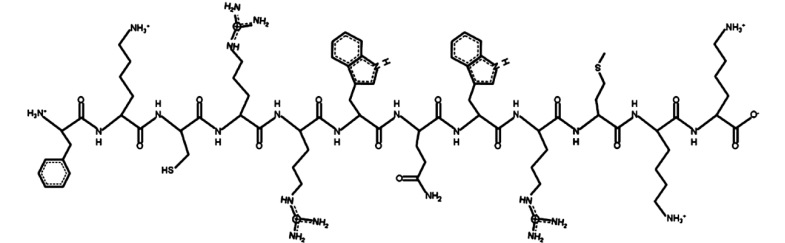
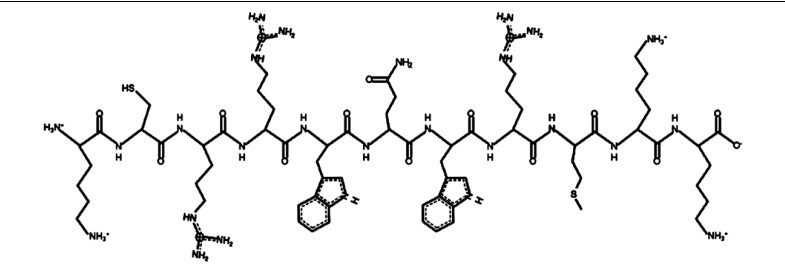
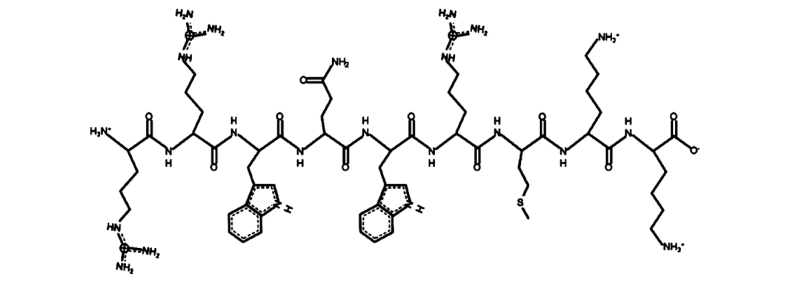
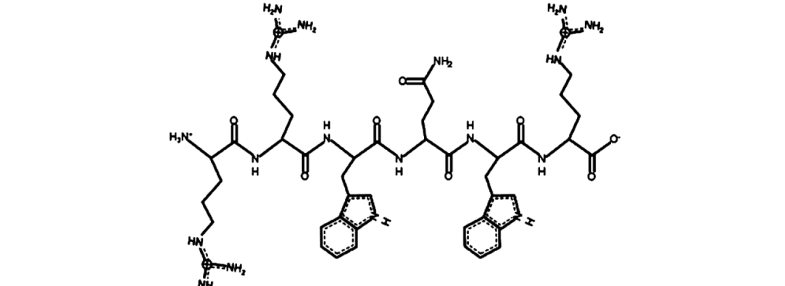
The pEGFP-N1 plasmid DNA containing the enhanced green fluorescent protein (*EGFP*) gene was purchased from Invitrogen. To prepare fluorescence-labeled DNA, pEGFP-N1 was labeled with the *LabelIT*[®] Cy5[™] Labeling Kit (Mirus Bio, Madison, WI, USA) according to the manufacturer's instructions.

2.3. Protein Internalization and Mechanistic Assay

In protein internalization experiments, A549 cells were treated with 10 μM of FITC-labeled lactoferricin derivatives at 37°C for 1 h, followed by Hoechst33342 staining following manufacturer's instructions (Invitrogen). The penetrating ability of FITC-labeled lactoferricin derivatives was monitored using fluorescent microscopy.

To determine cell line specific effects and the effect of the length of the FITC-labeled lactoferricin derivative, both A549 and HEK293FT cells were treated with 5 μM of FITC-labeled lactoferricin derivatives at 37°C for 1 h, and then analyzed by flow cytometry.

Table 1. Peptide list.

Peptides Name	M. W. (Daltons)	Purity (%)	Primary Sequence (N ^o →C ^o)	Chemical Structures
FITC-HR9	3503.95	87.31	CHHHHHRRRRRR RRRHHHHHC	
FITC-Lactoferricin	2253.72	88.84	CRRWQWRMKKL GC	
FITC-L12	2255.72	89.71	FKCRRWQWRMKK	
FITC-L11	2108.54	85.65	KCRRWQWRMKK	
FITC-L9	1877.23	89.87	RRWQWRMKK	
FITC-L6	1489.68	87.27	RRWQWR	

(Table 1) Contd....

Peptides Name	M. W. (Daltons)	Purity (%)	Primary Sequence (N ^o →C ^o)	Chemical Structures
FITC-L5a	1333.51	91.54	RRWQW	
FITC-L5b	1333.51	86.73	RWQWR	
FITC-L5a-digest	Uncertain	91.54	R+RWQW or RR+WQW	

To evaluate dose dependency, A549 cells were treated with 0, 1, 5, 10 or 30 μM of FITC-labeled lactoferricin derivative at 37°C for 1h. To study the effect of secondary structure in peptides of the same length, 10 μM FITC-L5a and FITC-L5b were incubated with A549 cells at 37°C for 1 h, followed by the analysis of fluorescent microscopy and flow cytometry.

In cellular transport assays, cells were treated with 2 μM of sodium fluoride (NaF; MedChemexpress; MCE, NJ, USA) [40, 41], 7.5 μM of filipin (Sigma-Aldrich, St. Louis, MO) [42], or 10 μM of cytochalasin (CytD; Sigma-Aldrich) [42] at 37°C, followed by incubation with either FITC-L5a or digested FITC-L5a for 1 h. To evaluate the role of macropinocytosis, cells were treated with 100 μM of 5-(*N*-ethyl-*N*-isopropyl)-amiloride (EIPA; Sigma-Aldrich) [42], followed by either FITC-L5a or digested FITC-L5a for 1 h. To evaluate the role of microtubules, cells were treated with 10 μM of nocodazole to depolymerize the microtubules, followed by incubation with either FITC-L5a or digested FITC-L5a for 1h [42].

For cargo delivery mediated by L5a, 10 μM FITC-L5a was pre-mixed with Cy5 labeled plasmid DNA at a N/P ratio of 12 to form complexes. A549 cells were treated with Cy5-DNA alone, FITC-L5a alone, or FITC-L5a/Cy5-DNA complexes at 37°C for 1 h. As a positive control, cells were treated with Lipofectamine (Invitrogen) premixed with DNA according to the manufacturer's instructions. Cells without any treatments were served as a negative control. In the mechanistic study, cells were pre-incubated with various

endocytic modulators at 37°C for 30 min, followed by FITC-L5a/Cy5-DNA complexes treatments for 1 h.

2.4. Confocal and Fluorescent Microscopy

Fluorescent and bright-field images were recorded using an AE31 inverted Epi-fluorescence microscope (Motic, Causeway Bay, Hong Kong) with an IS1000 eyepiece (Tucsen, Fujian, China) or a Nikon A1R⁺ confocal laser scanning microscope system (Nikon, Tokyo, Japan) using NIS-elements documentation software (Nikon). With the AE31 fluorescent microscope, excitation filters were set at 480/30 and 350/50 nm for green fluorescent protein (GFP) and blue fluorescent protein (BFP) channels, respectively. Emission filters were set at 535/40 and 460/50 nm for GFP and BFP channels, respectively. With the Nikon A1R⁺ confocal laser scanning microscope system, two solid-state lasers of 405 nm and 488 nm were used as the excitation source, and emission filters were set at 525/50 and 450/50 nm for the GFP and BFP channels, respectively. Bright-field images were used to observe cell morphology. The intensity of fluorescent images was quantified using UN-SCAN-IT software (Silk Scientific, Orem, UT, USA).

2.5. Flow Cytometric Analysis

Cells were seeded at a density of 1×10^5 per well in 24-well plates and incubated overnight in 500 μl /well of complete culture medium. Cells in the control and experimental groups treated with various FITC-labeled peptides were har-

vested and counted using a Cell Lab Quanta SC MPL flow cytometer (Beckman Coulter, Fullerton, CA, USA) or a Gallios Flow Cytometer (Beckman Coulter). To detect green fluorescence (FITC), excitation was set at 488 nm and emission at 515-545 nm using a FL1 filter. To detect red fluorescent probes (Cy5), excitation was set at 638 nm and emission at 650-670 nm performed as a FL3. Data were analyzed using CXP software (Beckman Coulter). Results are expressed as the percentage of the total cell population that displays fluorescence.

2.6. Zeta-potential and Particle Size Measurements

CPPs (10 μ M) were dissolved in double deionized water and vibrated to achieve homogeneity. Each solution was temperature-equilibrated at 25°C for 2 min in a capillary DTS1070 cuvette (Malvern Instruments, Worcestershire, UK). Sizes and zeta-potentials of peptides were measured using a Zetasizer Nano ZS and analyzed using Zetasizer software 6.30 (Malvern Instruments, Worcestershire, UK) [33, 42].

2.7. Cytotoxicity Assay

To assess the cytotoxicity of experimental treatments, A549 cells were seeded at a density of 1×10^4 per well in 96-well plates and incubated overnight in 200 μ l/well of full growth medium. Cells were treated with serum-free medium as a negative control, treated with 100% dimethyl sulfoxide (DMSO) as a positive control, or treated with FITC-L5a with an absence or presence of endocytosis modulators in serum-free RPMI medium at 37°C for 24 h. To measure the cytotoxicity of FITC-L5a/Cy5-DNA complexes, A549 cells were treated with complexes with an absence or presence of endocytosis modulators at 37°C for 24 h. The cells were washed with PBS at least three times before 1-(4,5-dimethylthiazol-2-yl)-3,5-diphenylformazan (MTT) dye was applied. Cell viability was measured using the colorimetric MTT dye reduction assay as previously described [36].

2.8. Statistical Analysis

Data are expressed as mean \pm standard deviations (SDs). Statistical comparisons between the control and experimental groups were undertaken using the Student's *t*-test. Mean values and SDs were calculated for each sample assayed in at least three independent experiments. The level of statistical significance was set at $P < 0.05$ (*) or 0.01 (**).

3. RESULTS

3.1. Cellular Internalization of Various Lactoferricin Derivatives

Lactoferricin derivatives containing different numbers of amino acids were designed (Table 1). Human A549 cells were treated with 10 μ M of FITC-labeled lactoferricin derivative peptides and then observed for cellular internalization using a fluorescent microscope (Fig. 1A). Strong green fluorescence was detected in all peptide-treated groups; little fluorescence was observed in negative controls (Fig. 1A). This indicates that FITC-HR9, FITC-lactoferricin, FITC-L12, FITC-L11, FITC-L9, FITC-L6, and FITC-L5a are highly active CPPs. Peptide sequences are shown in Fig. (1B).

3.2. Cell Type Specific Internalization of Various Lactoferricin Derivatives

To understand the effects of cell-specificity on cellular internalization, human lung cancer cells (A549) and viral-modified human embryonic kidney cells (HEK293FT) were incubated with various FITC-labeled lactoferricin derivatives (Fig. 2A). The uptake efficiencies of peptides were analyzed using a flow cytometer, and calculated as the fraction of fluorescent-positive cells. There was no significant difference between A549 and HEK293FT in the fraction of positive cells with any peptide (Fig. 2A; P 's > 0.05). To evaluate the influence of peptide length on cell internalization, the relationship between peptide length and protein internalization efficiency was analyzed using a scatter plot (Fig. 2B). Linear regressions in A549 generated an equation of $y = 3.2799(x) + 44.258$ with a Pearson's correlation coefficients of 0.4513; the corresponding equation in HEK293FT was $y = 3.5309(x) + 45.126$ with a correlation coefficient of 0.4961 (Fig. 2B). Thus, there is a low correlation between peptide length and internalization efficiency of lactoferricin-derivative CPPs.

Previous studies indicated that the penetration abilities of CPPs and their entry mechanisms were concentration dependent [43, 44]. To determine the effects of concentration in various lactoferricin derivatives, A549 cells were treated with FITC-labeled peptides at 0, 1, 5, 10, and 30 μ M (Fig. 2C). FITC-HR9, FITC-Lactoferricin, FITC-L12, FITC-L11, FITC-L6, and FITC-L5a were internalized at the concentration of 1 μ M; no significant differences in concentration-dependence were observed (Fig. 2C; P 's > 0.05). Accordingly, cell type, peptide length, and concentrations are not the primary factors governing protein internalization efficiency.

3.3. Influence of Peptide Secondary Structure on Cellular Internalization

To further identify key factors governing cellular uptake in peptides, the primary sequence of a lactoferricin-derived pentapeptide was altered. FITC-L5a differed from FITC-L5b in position of arginine. This slight difference in sequence caused a marked difference in cellular internalization (Fig. 3A). Strong green fluorescence was detected in the cells treated with FITC-L5a, while little green fluorescence was observed in cells treated with FITC-L5b (Fig. 3A). Internalization of FITC-L5a and FITC-L5b were further quantified by flow cytometry. The population of positive cells in FITC-L5a treated groups almost reached 100% (Fig. 3B), while the fraction of positive cells in FITC-L5b treated groups was at a much lower level (Fig. 3B; $P < 0.01$). Thus, the internalization abilities of FITC-L5a and FITC-L5b were quite distinct, although they shared the same length and composition of amino acids.

To identify physical properties of FITC-L5a and FITC-L5b which might determine cell internalization, zeta-potential, particle size, and helical structure of peptides were examined. FITC-HR9, FITC-L5a, and FITC-L5b were analyzed in aqueous solutions at pH 7. FITC-HR9 with strongly positive charges served as a positive control [33]. The zeta-potential of FITC-L5b was electro negative at pH 7 (-0.8 ± 1.2 mV), while the zeta-potential of FITC-L5a was 1.5 ± 0.7 mV (Fig. 3C).

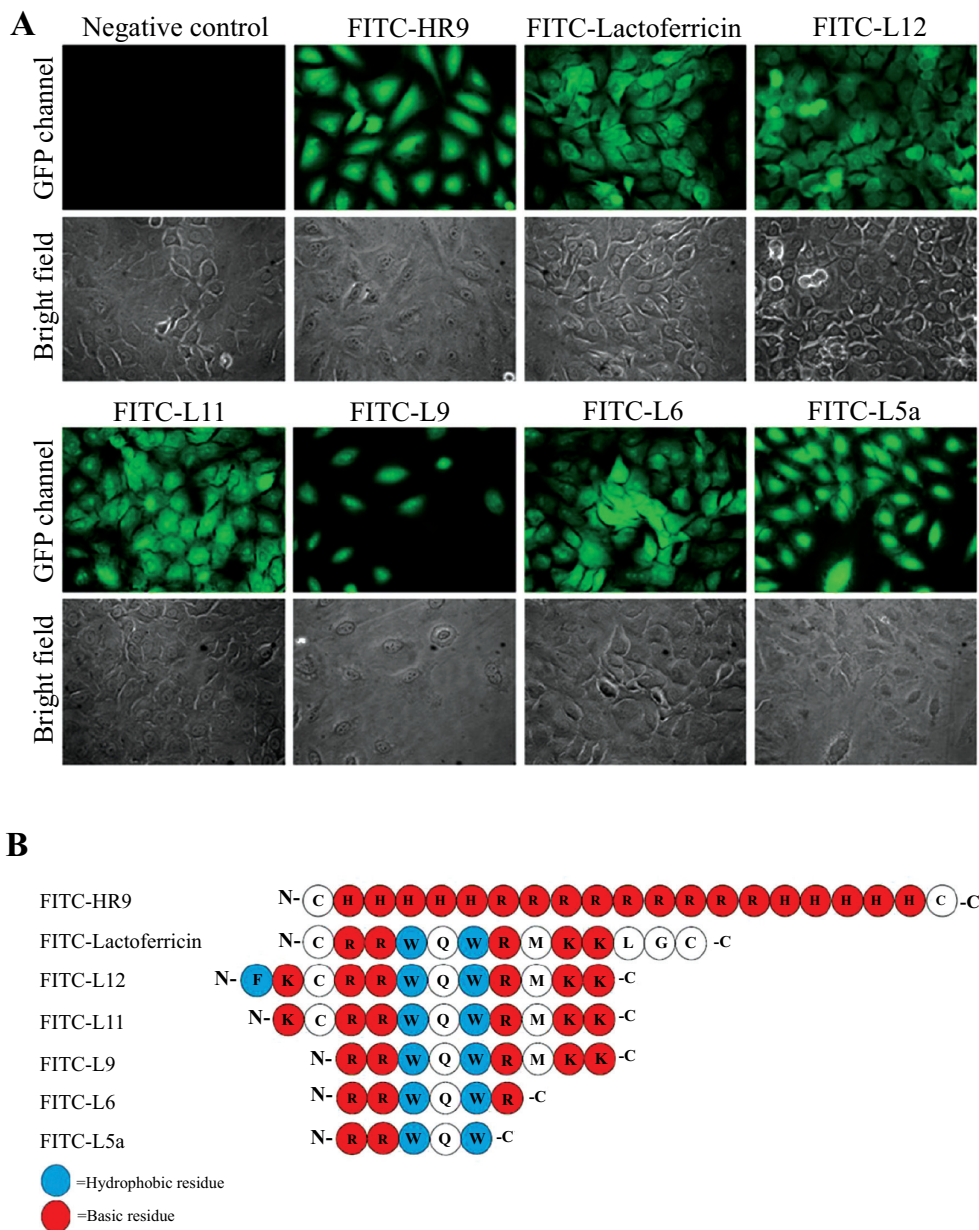


Fig. (1). Cellular internalization of various lactoferricin derivative peptides. A) 549 cells were treated with various length of lactoferricin derivatives labeled with FITC in the concentration of 10 μ M for 1 h. B) Cells without any treatments were served as the negative control, and treated with 10 μ M FITC-HR9 as the positive control. All images were observed with a Motic AE31 fluorescent microscope at the magnification of 400 \times . GFP channel displayed the intracellular distribution of peptides, and bright fields revealed the cell morphologies.

All three peptides were of similar sizes: 164.09 ± 11.6 nm, 112.38 ± 72.8 nm, and 101.97 ± 96.8 nm (Fig. 3C; P 's > 0.05). These results agree with our previous finding that the electrostatic interactions can be a predictor of internalization efficiency within the charge range tested [33, 42, 45].

To explore the differences in spatial architecture that might contribute to differences in internalization efficiency of FITC-L5a and FITC-L5b, Helical wheel progress of SeqWeb v3.1.2 software was used to recognize amphiphilic regions in peptides [46, 47]. Peptide sequences of FITC-L5a and FITC-L5b were plotted as helical wheels set in 18 steps

and 5 turns of output section (Fig. 3D; left). Helical wheel projections converted into quadrantal and rota-schematic diagrams showed the differing distribution of the charged and hydrophobic sections of the three-dimensional structures (Fig. 3D; middle and right). Symmetry of basic residues in FITC-L5a generating the homogeneously positive sheath of structures in space diverged from the hemispherical features of charged/hydrophobic sections in FITC-L5b (Fig. 3D; middle and right). These results confirmed previous descriptions of differences in zeta potential between FITC-L5a and FITC-L5b.

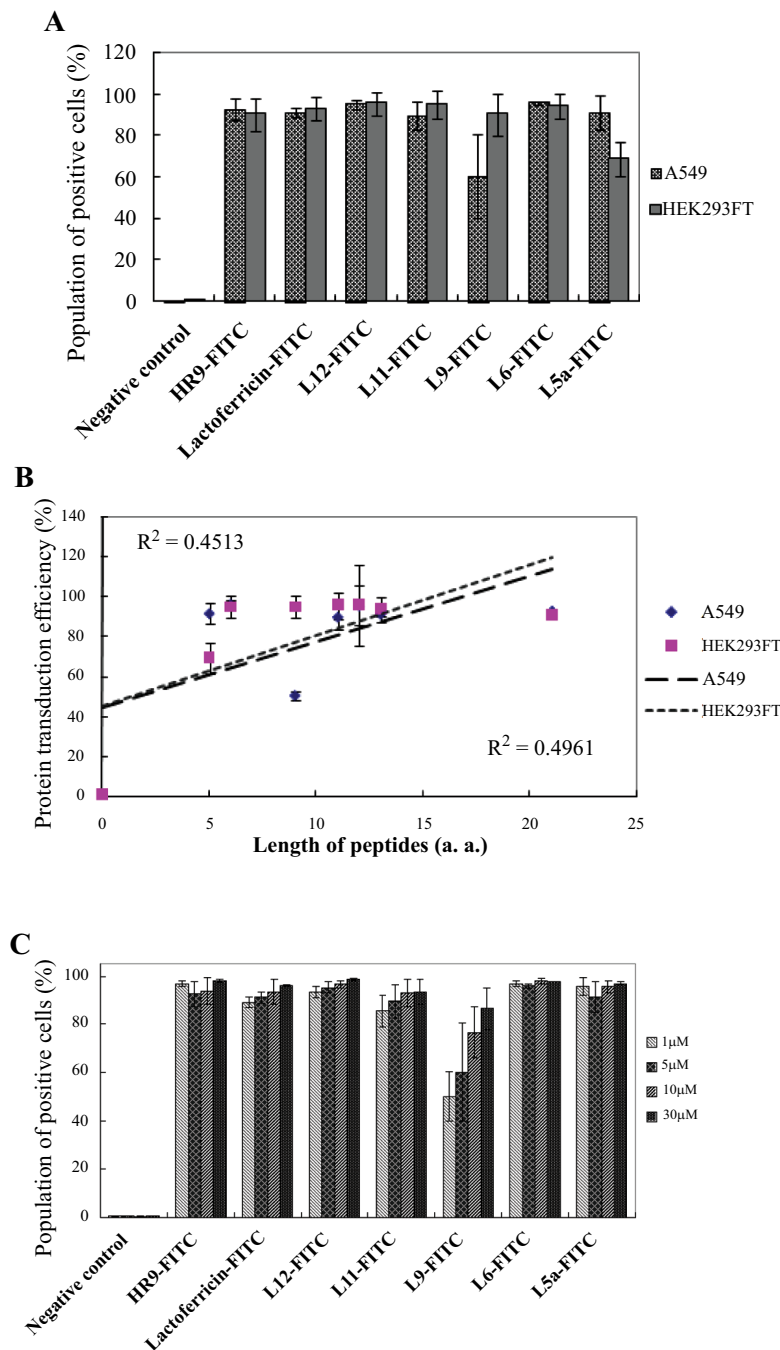


Fig. (2). Factors involved in cellular internalization of lactoferricin-derived peptides. (A) Cell type-specific effects in cellular internalization of different lactoferricin-derived peptides. Both HEK293FT cells and A549 cells were treated with 5 μ M FITC labeled lactoferricin derivatives for 1 h and the internalization efficiency was measured with the flow cytometry. Cells without any treatment served as negative controls and cells treated with FITC-HR9 as positive controls, respectively. (B) Correlation between protein transduction efficiency and the lengths of lactoferricin-derived peptides. Five micromolar of different lengths of peptides were incubated with HEK293FT and A549 cells, respectively, and their protein transduction efficiencies were correlated with peptide lengths. Blue rhombi and pink squares in the scatter plot indicated the results of the correlation between peptide lengths and efficiencies in A549 and HEK293FT, respectively. The pecked line and dotted line revealed the linear regressions in A549 and HEK293FT, respectively. Pearson correlation coefficients (R) for A549 were shown at the up-left of the scatter plot ($R^2 = 0.4513$) and at the down-right position for HEK293FT ($R^2 = 0.4961$). (C) Dosage-dependent effects on cellular internalization. FITC-labeled peptides at 1, 5, 10, and 30 μ M concentrations were incubated with A549 cells for 1 h and cellular internalizations were analyzed using a flow cytometer. Cells without any treatment served as negative controls while cells treated with FITC-HR9 as positive controls.

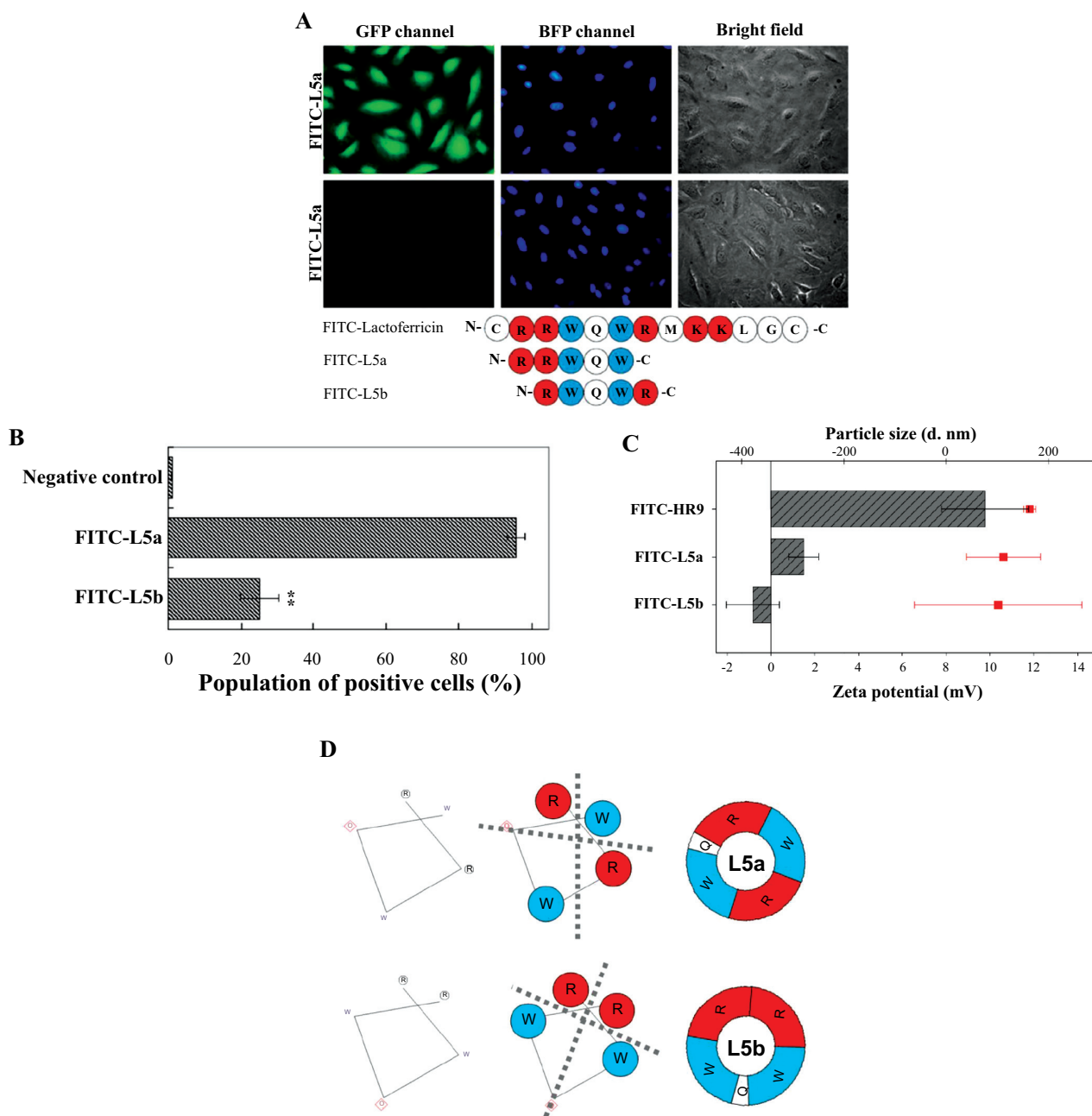


Fig. (3). Comparison of lactoferricin-derived pentapeptides with different primary and secondary structures. (A) Microscopy of cellular internalization in two different sequences of pentapeptides. A549 cells were treated with 10 μ M FITC-labeled L5a and L5b for 1 h, respectively. GFP channels and bright fields revealed the distributions of FITC-labeled L5a and L5b, as well as cell morphologies. All images are obtained using a Motic AE31 fluorescent microscope with a magnification of 400 \times . The primary architectures of lactoferricin, L5a, and L5b sequences were shown below images. Basic residues were revealed in red and hydrophobic amino acids were in cyan. (B) Flow cytometry analysis of cellular internalization in lactoferricin-derived pentapeptides. 10 μ M FITC-labeled L5a and L5b were incubated with A549 cells for 1 h, and the fraction of cells internalizing peptides was determined by flow cytometry. Cells without any treatment served as negative controls. Statistical comparisons between FITC-L5a and FITC-L5b were performed by student's *t* test. Significant differences set at $P < 0.01$ (**). Data of each treatment group are presented as mean \pm SD from seven independent experiments. (C) Zeta potential and particle size analyses of peptides. FITC-HR9, FITC-L5a, and FITC-L5b were dissolved in double deionized water and measured for both zeta potential and sizes using a Zetasizer Nano ZS. FITC-HR9 served as a positive control. Data of each treatment group are presented as mean \pm SD from five independent experiments. (D) Comparison of secondary structures in L5a and L5b in helical wheel. Helical wheel software was used for L5a and L5b helical structures prediction (left). Quadrantal diagrams and rota-schematic diagrams simulated the distributions of positive-charges and hydrophobicity (middle and right). Basic amino acids were shown in red and hydrophobic amino acids were in cyan.

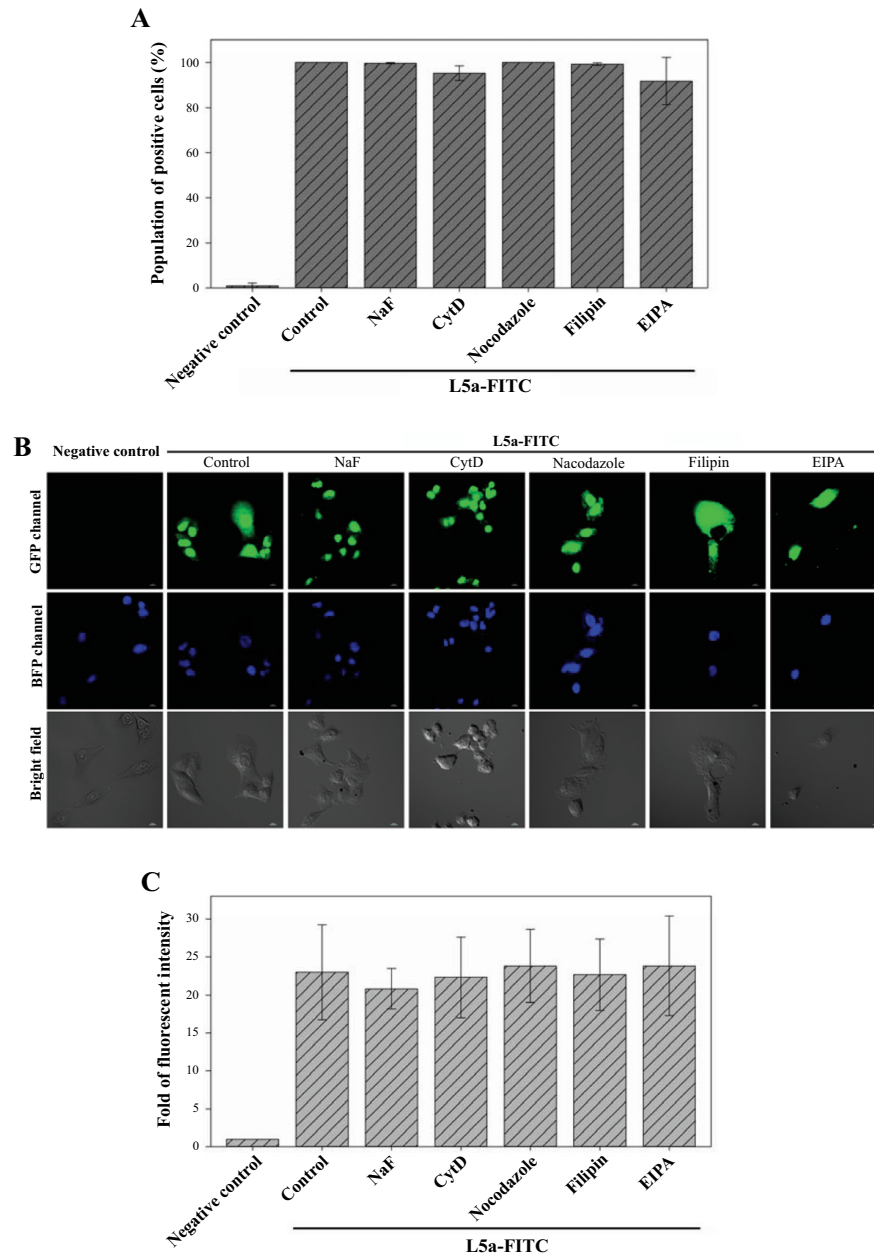


Fig. (4). Mechanisms of FITC-L5a cellular internalization. (A) Flow cytometric analysis. A549 cells were treated with endocytosis inhibitors for 30 min before incubation with FITC-L5a. After protein transduction procedure, the fraction of cells internalizing the FITC-L5a was analyzed with a flow cytometer. Statistical comparisons to the control of FITC-L5a were performed by student's *t* test. Significant differences were set at $P < 0.05$ (*) and $P < 0.01$ (**). Data of each treatment group are presented as mean \pm SD from four independent experiments. (B) Confocal microscopy of cellular internalization of FITC-L5a with different inhibitor treatments. Cells were stained with Hoechst33342. GFP, BFP channels and bright fields revealed the distributions of FITC-labeled L5a, nuclei, and cell morphologies. Images were obtained by a Nikon A1R+ confocal laser microscope system with a magnification of 800 \times . (C) Quantification of the cellular internalization of FITC-L5a. The fluorescent intensity of FITC-L5a was quantified using the UN-SCAN-IT software. Each experimental group was compared with the control of FITC-L5a and statistical differences were calculated using the Student's *t*-test. Significant differences were set at $P < 0.05$ (*) and $P < 0.01$ (**). Data of each treatment group are presented as mean \pm SD from five independent experiments.

As FITC-L5a peptide was efficiently taken up by cells, we investigated the mechanism of its cellular internalization. Cells were treated with cellular process modulators before adding FITC-L5a, and then analyzed with flow cytometry and confocal microscopy to estimate the fraction of cells

displaying with FITC fluorescence (Fig. 4). Cells with FITC-L5a peptide displayed high efficiency of protein internalization in flow cytometric data (Fig. 4A). Disruption of energy-dependent cellular uptake processes by sodium fluoride did not compromise cellular uptake of FITC-L5a, (Fig. 4A;

99.63 ± 0.3% vs. 99.99 ± 0.02%). There was no difference in uptake in the presence or absence of the F-actin rearrangement inhibitor (CytD) (Fig. 4A; 95.28 ± 3.2%; $P > 0.05$). Nocodazole and filipin were used to investigate clathrin- and caveolae-related cellular uptake. Cell populations with FITC fluorescence were 99.98 ± 0.02% and 99.19 ± 0.6% in the nocodazole or filipin treated groups, respectively (Fig. 4A). We treated cells with macropinocytosis inhibitor EIPA. EIPA slightly reduced the fluorescent population in FITC-L5a treated cells, but no significant difference was observed (Fig. 4A; 91.77 ± 16.5%; $P > 0.05$). Thus, FITC-L5a entry did not appear to involve endocytosis pathways.

Confocal microscopy was used to further confirm the mechanism of cellular internalization of FITC-L5a. Various intensities of green fluorescence were detected in cells treated with FITC-L5a in an absence (control) or presence of endocytic modulators (Fig. 4B). Interestingly, FITC-L5a in each treated group colocalized with nuclei (Fig. 4B). The change of fluorescent intensity was quantified from signals of GFP channel in Fig. 4B. Results from these analyses (Fig. 4C) were in agreement with those from the flow cytometry (Fig. 4A). The application of modulators did not lead to significant differences in comparison with the control ($P > 0.05$). Accordingly, it is possible that direct membrane translocation is the pathway for FITC-L5a uptake.

To further confirm the importance of the secondary structures in FITC-L5a in cellular internalization, incompletely symmetric architectures of peptides were produced by tryptic digestion. Cells were treated with digested FITC-L5a in the absence or presence of endocytic modulators, and analyzed by both flow cytometry and confocal microscopy (Fig. 5). The fraction of FITC positive cells treated with tryptic FITC-L5a, but without an endocytic modulator (the control), was reduced to 72.03 ± 10.4% (Fig. 5A). All groups treated with chemical modulators had reduced in uptake compared to the control (Fig. 5A; P 's < 0.05 or < 0.01). Energy depletion with sodium fluoride diminished FITC-L5a uptake to the greatest effect. However, green fluorescence was also significantly decreased in cells treated with FITC-L5a in the presence of CytD, nocodazole, filipin, and EIPA (Fig. 5B and 5C; P 's < 0.05 or < 0.01). Significant differences were not observed among these groups of inhibitor treatments (Fig. 5A and 5C; P 's > 0.05). These results indicate that tryptic FITC-L5a enter cells via a classical energy-dependent endocytosis pathway (Fig. 5). We conjecture that the mechanism of cellular internalization might have been altered as a result of the conformational incompleteness of FITC-L5a. A symmetrically positive-charged architecture of FITC-L5a affecting the zeta potential and electrostatic interactions with plasma membranes might be a key factor contributing to high internalization efficiency and direct membrane translocation.

3.4. Mechanism of L5a/DNA Complex Entry into Cells

To determine whether DNA can be delivered into cells by L5a, A549 cells were treated with FITC-L5a/Cy5-DNA complexes at the N/P ratio 12, and DNA transfection efficiency was evaluated by flow cytometry. Cells treated with Lipofectamine/Cy5-DNA and FITC-L5a alone served as the positive controls for DNA transfection and CPP internalization, respectively. No signal was detected in cells treated

with Cy5-labeled DNA alone (Fig. 6A). However, red and green fluorescence was detected in cells treated with Lipofectamine/Cy5-DNA and FITC-L5a alone, respectively (Fig. 6A). In the FITC-L5a/Cy5-DNA complex group, both red and green fluorescence were detected, indicating that FITC-L5a not only penetrated cells by themselves but also took Cy5-DNA as cargo through plasma membrane (Fig. 6A). These results confirmed our previous outcome that L5a possesses the ability to transport DNA into cells. To determine the mechanism of cellular uptake of FITC-L5a/Cy5-DNA complexes, cells were treated with different endocytic modulators prior to exposure to FITC-L5a/Cy5-DNA complexes (Fig. 6B). Cells were treated with sodium fluoride to deplete energy-dependent endocytic pathways, CytD to block F-actin rearrangements, nocodazole to induce microtubule depolymerization, filipin to sequester lipid, or EIPA to specifically inhibit macropinocytosis. Results indicated that none of these endocytic modulators affect the delivery of FITC-L5a/Cy5-DNA complexes into cells (Fig. 6B; P 's > 0.05). These results suggest that both FITC-L5a and FITC-L5a/Cy5-DNA complexes utilize a direct membrane translocation pathway.

3.5. Cytotoxicity

The MTT assay was used to determine the effect of FITC-L5a penetration and FITC-L5a/Cy5-DNA complexes delivery on cell viability. Cells were treated with either FITC-L5a (Fig. 7A) or FITC-L5a/Cy5-DNA complexes (Fig. 7B) in the absence or presence of endocytosis inhibitors. Cells treated with EIPA group displayed no significant reduction of viability (Fig. 7). Only cells treated with 100% DMSO (positive control) had significantly reduced viability. None of the materials used in this study caused cytotoxicity, indicating that FITC-L5a would be a safe vehicle for drugs and gene delivery.

4. DISCUSSION

In this study, we demonstrate that the secondary structure of FITC-L5a, the shortest lactoferricin derivative that is active as a CPP, is the primary factor governing cellular internalization (Figs. 3-5). Six lactoferricin derivatives of various lengths exhibit high internalization efficiency in various cell lines and concentrations, indicating that peptide length, treatment amounts, and cell types are not major factors controlling cellular internalization (Figs. 1 and 2). FITC-L5b constructs containing similar primary structure but different secondary structures display distinct penetration abilities (Fig. 3). FITC-L5a possesses minimal cytotoxicity, and could serve as a nano-drug delivery system [33].

FITC-L5a is not the only CPP that enters cells by direct membrane translocation. In 2011, we demonstrated that HR9 interact with luminescent semiconductor nanoparticle QDs, and these HR9/QD complexes can enter cells without using an energy-dependent endocytosis pathway [35]. Physical and chemical inhibitors of membrane transport do not interfere with HR9's ability to deliver genes into cells [26]. Cell penetration efficiency makes HR9 an ideal vector for delivering genes and nanomaterials to cells of various species [21, 22, 26, 27, 35, 48]. We also reported that the pentapeptide L5a can deliver genes that are expressed by cells [33]. In agreement

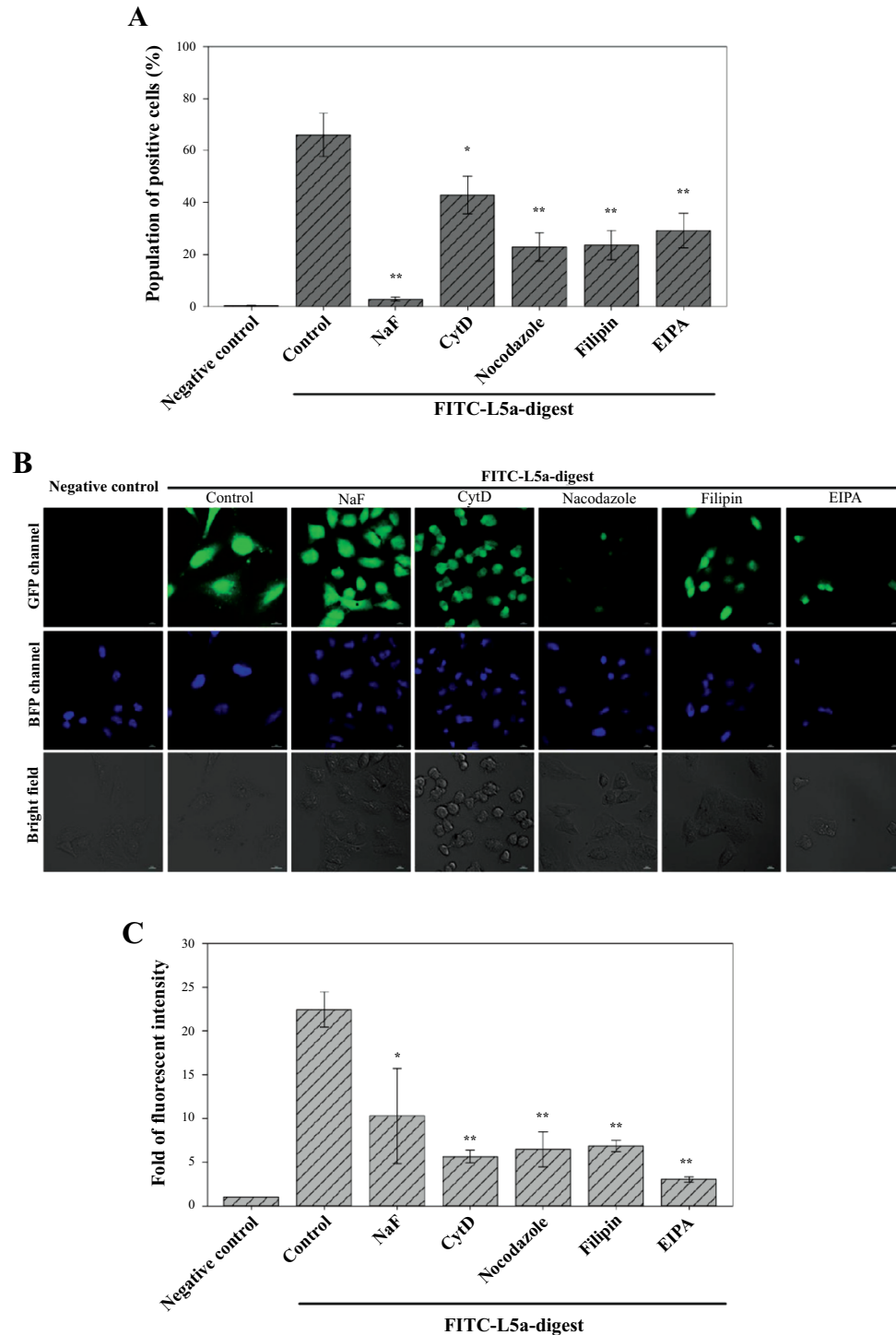


Fig. (5). Mechanisms of uptake of conformational destroyed FITC-L5a. (A) Flow cytometric analysis of FITC-L5a uptake. Incomplete conformation of FITC-L5a was formed by trypsin digestion and incubated with A549 cells in the presence or absence of different endocytosis inhibitors for 30 min. The fraction of cells internalizing the digested FITC-L5a was analyzed with a flow cytometer. (B) Confocal microscopy of cellular internalization of digested FITC-L5a in different inhibitor treatments. After all treatments described in (A), cells were then stained with Hoechst33342. GFP, BFP channels and bright fields revealed the distributions of digested FITC-L5a, nuclei, and cell morphologies. Images were obtained by a Nikon A1R+ confocal laser microscope system with a magnification of 800×. (C) Quantification of the cellular internalization of tryptic FITC-L5a. The fluorescent intensity of was quantified using UN-SCAN-IT software. Each experiment group was compared with the tryptic FITC-L5a control group and statistical differences were calculated using the Student's *t*-test. Significant difference was set at $P < 0.05$ (*) and $P < 0.01$ (**). Data of each treatment group are presented as mean \pm SD from five independent experiments.

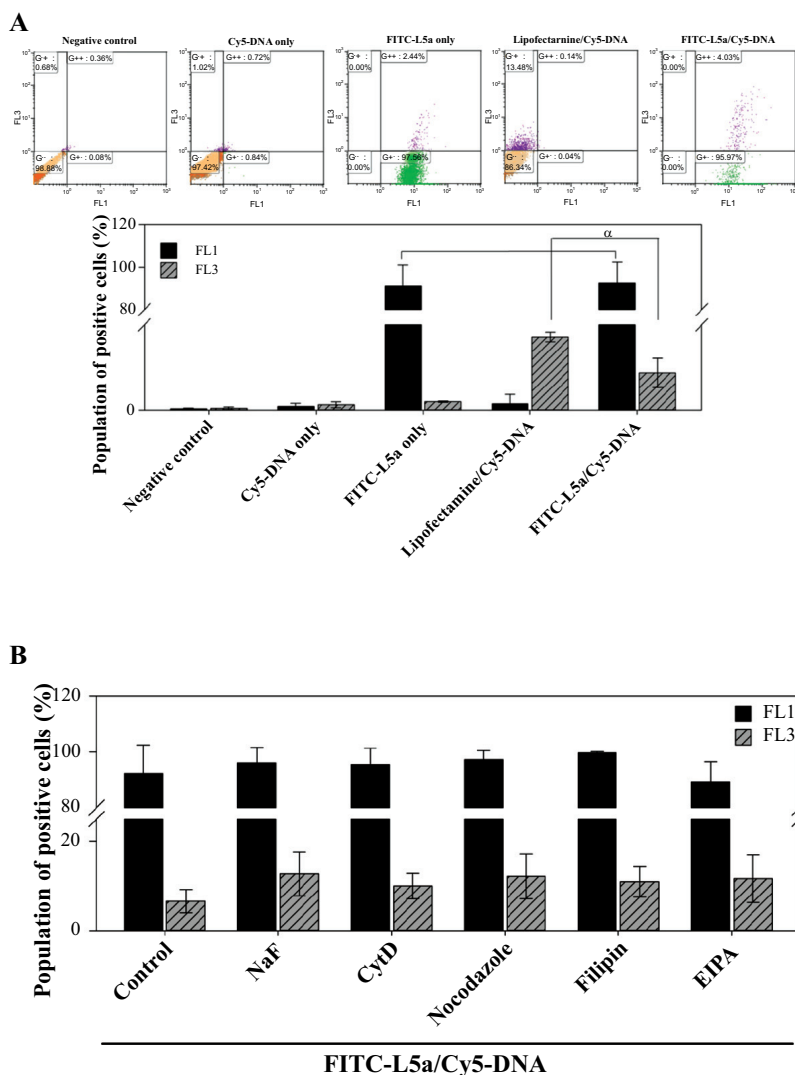


Fig. (6). Mechanisms of FITC-L5a/Cy5-DNA complexes cellular uptake. (A) Comparison of transfection efficiency. A549 cells were incubated with Cy5-DNA only, FITC-L5a only, lipofectamine/Cy5-DNA, and FITC-L5a/Cy5-DNA complexes at 37°C for 1 h, respectively. Cy5 labeled DNA transfection efficiency was evaluated by flow cytometry. Green fluorescence detection for FITC-L5a internalization was reported as FL1, and red fluorescence for Cy5-DNA transfection was indicated as FL3. (B) Mechanisms of FITC-L5a/Cy5-DNA complexes delivery into A549 cells. FITC-L5a and Cy5-DNA were mixed with the N/P ratio of 12 to form complexes. Cells were treated with complexes in the absence or presence of endocytosis inhibitors at 37°C for 1 h. Populations of transfected cells were evaluated by flow cytometry. FL1 performed the internalization efficiency of FITC-L5a, and FL3 performed the transfection efficiency of Cy5-DNA. Data of each treatment group were presented as mean \pm SD from three independent experiments in each treatment group. Statistics was performed by Student's *t*-test. Significant difference was set at $P < 0.05$.

with the present study, L5b exhibited weak penetration ability, and should not be classified as a CPP [33]. Fang *et al.* reported that bLFCin₆ (RRWQWR, corresponding to L6 in the present study) possessed cell-penetrating properties, but not CPP₅ (RWQWR, corresponding to L5b in the present study) [32]. Our results with L5a and L5b (Fig. 3) are consistent with our earlier observations [33]. Both L5a and L5b contain the same number of amino acids, with only one arginine at a different position in sequence. This slight difference has significant functional consequences. An antiparallel beta-sheet structure adopted as a helical or sheet-like conformation is important for lactoferrin interaction with cel-

lular membranes, as indicated by nuclear magnetic resonance [49]. Lactoferrin efficiency of uptake was related to the location of the beta-strand in relation to the positive charges [50]. The six peptides studied in the present work were derived from lactoferrin [33, 51]. Although there is little information available on the structure of L6, it is likely that L6 conserves the antiparallel beta-sheet structure, and transforms its structure to helical conformation when interacting with the cell membrane. The mechanism of L6-mediated delivery of siRNA into HeLa cells is by macropinocytosis [32]. In contrast, L5a and L5a/DNA complexes enter cells via direct membrane translocation (Fig. 4 and Fig. 6B). This

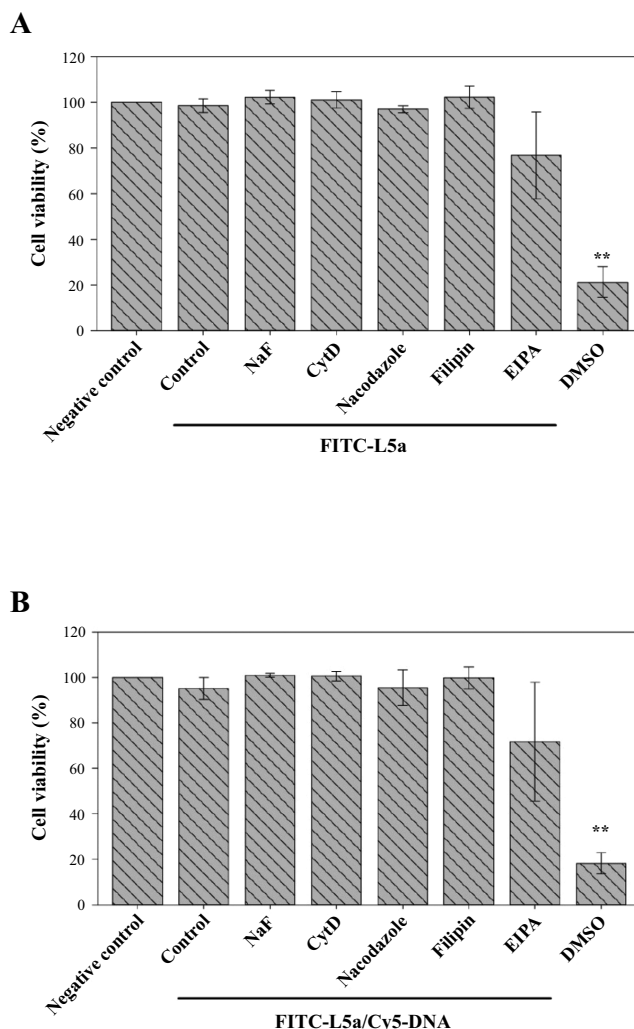


Fig. (7). Cytotoxicity of FITC-L5a and FITC-L5a/Cy5-DNA complexes with inhibitors. **(A)** Cytotoxicity of FITC-L5a and various inhibitors. Human A549 cells were treated with 10 μ M FITC-L5a in the absence or presence of endocytosis inhibitors at 37°C for 24 h. The colorimetric MTT assay was used to evaluate cell viability after treatments of FITC-L5a and various endocytic modulators. Cells treated with serum-free medium and 100% DMSO at 37°C for 24 h served as negative and positive controls, respectively. **(B)** Cytotoxicity of FITC-L5a/Cy5-DNA complexes and various inhibitors. Cells were treated with FITC-L5a/Cy5-DNA complexes at the N/P ratio of 12 in the absence or presence of endocytosis inhibitors at 37°C for 24 h. Cells treated with serum-free medium and 100% DMSO at 37°C for 24 h served as negative and positive controls, respectively. Data of each treatment group were presented as mean \pm SD from three independent experiments. Significant difference was set at $P < 0.01$ (**).

difference might be due to a conformational change. The α -helices in FITC-L5a suggested by two-dimensional projections of helical wheels provide a reasonable explanation for this phenomenon. Positive charges evenly surrounding the periphery of L5a differ from the distributions of positive charges in L5b, and are likely to contribute to penetration efficiency (Fig. 3). Comparison of all of the structures of lactoferricin derivatives from L12 to L6 indicates that positive charges arranged around the periphery of peptides is positively correlated with penetration efficiency (Fig. 8A). In contrast, the positive charges of L4 and L5b, both nonCPPs [33], were present on only a small portion of the circles (Fig. 3D and 8B). Previously, we identified direct membrane translocation as the entry mechanism of HR9 peptide-mediated cellular internalization [26, 35]. Here, we use the

HelicalWheel progress of SeqWeb v3.1.2 software to model the HR9 peptide structure. We found dense and consistent positive charges located around the periphery of active peptides without any intervals (Fig. 8A). These findings are consistent with the hypothesis presented in this study: peptides with abundant and central symmetrical positive charges distributed along their peripheries possess high efficiency of cellular internalization mediated by direct membrane translocation.

Studies indicate that various factors influence cellular internalization of peptides and their ability to deliver cargoes. The primary factor for transduction efficiency is the composition of the CPP [18, 24, 44, 52]. Other factors include the type of cells targeted, the concentrations of CPPs,

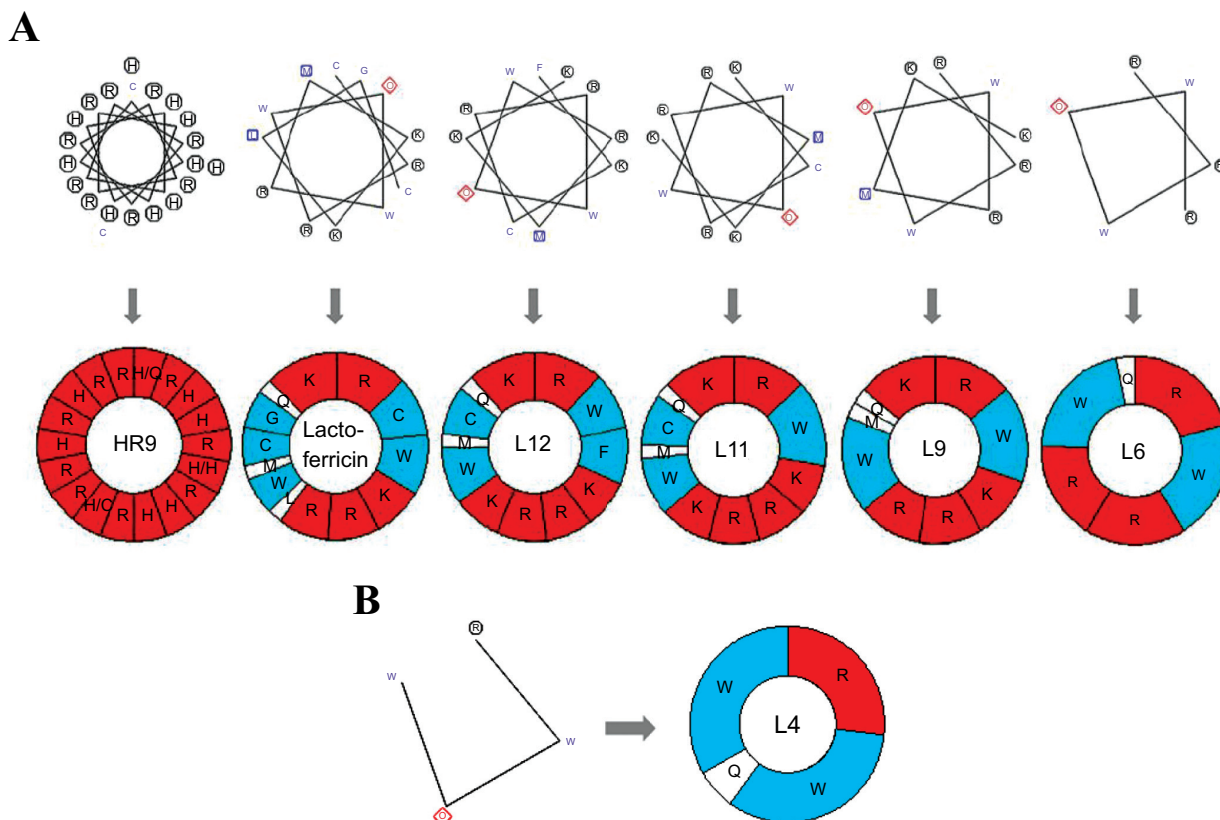


Fig. (8). Secondary structures of various lactoferricin derivative peptides in helical wheel. (A) Helical wheel software was used for CPP helical structure prediction. HR9, lactoferricin, L12, L11, L9, and L6 exhibited the properties of CPPs and rotaschematic diagrams clarified the symmetrical distributions of positive-charges and hydrophobicity **(B)** Prediction of L4 helical structures with Helical wheel software. Rotaschematic diagrams illustrated a small portion of positive-charges distribution. Basic amino acids were shown in red and hydrophobic amino acids were in cyan.

the methods of cargoes conjugation, and the chemical and physical properties of the cargoes [16, 19, 43-45, 52]. Recently, the effect of zeta potential on the efficiency of protein transductions has been considered [33, 45]. The present study emphasizes the role of spatial architectures of positive charges, and demonstrates a correlation between zeta potential and the distribution of positive charge in helical wheels. Two-dimensional projections of helical wheels have been widely used in projections of CPP properties [47]. For example, Oct4-PTD and penetratin display conservation of a helical wheel projection, rather than a conservation of the primary sequences [46]. The present study offers additional insight into the relationship between secondary structure and penetrating efficiency, as well as the roles of secondary peptide structures of peptides in cellular internalization.

CONCLUSION

High penetration efficiency was exhibited with bovine lactoferricin FITC-L5a (RRWQW), but not with the isomeric peptide FITC-L5b (RWQWR). Helical wheel projections revealed that FITC-L5a contains a homogenous distribution of symmetrically positive charges in space with basic and hydrophobic residues occupying opposite sections of the wheels. Complete structures of FITC-L5a entered cells by

direct membrane translocation, yet the entry mechanism converted to endocytosis upon structural disruption. Direct membrane translocation was also utilized in FITC-L5a/Cy5-DNA complex delivery. FITC-L5a alone or in combination with other endocytic modulators was not cytotoxic. Thus, FITC-L5a one of the shortest functional CPPs, enters cells via direct membrane translocation, and could serve as an efficient and safe vehicle for drug delivery.

LIST OF ABBREVIATIONS

BFP	=	Blue fluorescent protein
CPP	=	Cell-penetrating peptide
CytD	=	Cytochalasin D
EIPA	=	5-(<i>N</i> -ethyl- <i>N</i> -isopropyl)-amiloride
FITC	=	Fluorescein isothiocyanate
GFP	=	Green fluorescent protein
HIV-1	=	Human immunodeficiency virus type 1
HR9	=	Histidine-rich nona-arginine
MTT	=	1-(4,5-dimethylthiazol-2-yl)-3,5-diphenylformazan
NaF	=	Sodium fluoride
PBS	=	Phosphate buffered saline

PTD = Protein transduction domain
 QDs = Quantum dots
 siRNA = Small interfering RNA
 Tat = Transactivator of transcription.

ETHICS APPROVAL AND CONSENT TO PARTICIPATE

Not applicable.

HUMAN AND ANIMAL RIGHTS

No Animals/Humans were used for studies that are base of this research.

CONSENT FOR PUBLICATION

Not applicable.

CONFLICT OF INTEREST

The authors declare no conflict of interest, financial or otherwise.

ACKNOWLEDGEMENTS AND FUNDING

We are grateful to Dr. Hwei-Hsien Chen (National Health Research Institutes, Taiwan) for the generous provision of the HEK293FT cells. We thank Drs. Chia-Liang Cheng (National Dong Hwa University, Taiwan) for performing the zeta-potential measurements. This work was supported by the Grant No. MOST 105-2320-B-259-002-MY3 (to H.-J. L.) and the Grant No. MOST 104-2311-B-320-002- as well as Grant No. MOST 106-2320-B-320-001-MY3 (to B. R. L.) from the Ministry of Science and Technology, Taiwan.

REFERENCES

- De Jong, W.H.; Borm, P.J. Drug delivery and nanoparticles: applications and hazards. *Int. J. Nanomed.*, **2008**, *3*(2), 133-149.
- Tiwari, G.; Tiwari, R.; Sriwastawa, B.; Bhati, L.; Pandey, S.; Pandey, P.; Bannerjee, S.K. Drug delivery systems: An updated review. *Int. J. Pharm. Investig.*, **2012**, *2*(1), 2-11.
- Zhang, Y.; Chan, H.F.; Leong, K.W. Advanced materials and processing for drug delivery: The past and the future. *Adv. Drug Deliv. Rev.*, **2013**, *65*(1), 104-120.
- Allen, T.M.; Cullis, P.R. Drug delivery systems: Entering the mainstream. *Science*, **2004**, *303*(5665), 1818-1822.
- Johnstone, T.C.; Suntharalingam, K.; Lippard, S.J. The next generation of platinum drugs: Targeted Pt(II) agents, nanoparticle delivery, and Pt(IV) prodrugs. *Chem. Rev.*, **2016**, *116*(5), 3436-3486.
- Zhao, M.X.; Zhu, B.J. The research and applications of quantum dots as nano-carriers for targeted drug delivery and cancer therapy. *Nanoscale Res. Lett.*, **2016**, *11*(1), 207.
- Frandsen, J.L.; Ghandehari, H. Recombinant protein-based polymers for advanced drug delivery. *Chem. Soc. Rev.*, **2012**, *41*(7), 2696-2706.
- Lonn, P.; Dowdy, S.F. Cationic PTD/PPP-mediated macromolecular delivery: charging into the cell. *Expert Opin. Drug Deliv.*, **2015**, *12*(10), 1627-1636.
- van den Berg, A.; Dowdy, S.F. Protein transduction domain delivery of therapeutic macromolecules. *Curr. Opin. Biotechnol.*, **2011**, *22*(6), 888-893.
- Vives, E.; Brodin, P.; Lebleu, B. A truncated HIV-1 Tat protein basic domain rapidly translocates through the plasma membrane and accumulates in the cell nucleus. *J. Biol. Chem.*, **1997**, *272*(25), 16010-16017.
- Moutal, A.; Francois-Moutal, L.; Brittain, J.M.; Khanna, M.; Khanna, R. Differential neuroprotective potential of CRMP2 peptide aptamers conjugated to cationic, hydrophobic, and amphipathic cell penetrating peptides. *Front. Cell Neurosci.*, **2015**, *8*, 471.
- Guo, Z.; Peng, H.; Kang, J.; Sun, D. Cell-penetrating peptides: Possible transduction mechanisms and therapeutic applications. *Biomed. Rep.*, **2016**, *4*(5), 528-534.
- Gautam, A.; Singh, H.; Tyagi, A.; Chaudhary, K.; Kumar, R.; Kapoor, P.; Raghava, G.P. CPPsite: A curated database of cell penetrating peptides. *Database (Oxford)*, **2012**, *2012*, bas015.
- Huang, Y.W.; Lee, H.J.; Tolliver, L.M. Aronstam, R.S. Delivery of nucleic acids and nanomaterials by cell-penetrating peptides: Opportunities and challenges. *Biomed. Res. Int.*, **2015**, *2015*, 834079.
- Chang, M.; Chou, J.C.; Lee, H.J. Cellular internalization of fluorescent proteins via arginine-rich intracellular delivery peptide in plant cells. *Plant Cell Physiol.*, **2005**, *46*(3), 482-488.
- Hu, J.W.; Liu, B.R.; Wu, C.Y.; Lu, S.W.; Lee, H.J. Protein transport in human cells mediated by covalently and noncovalently conjugated arginine-rich intracellular delivery peptides. *Peptides*, **2009**, *30*(9), 1669-1678.
- Liu, B.R.; Huang, Y.W.; Chiang, H.J.; Lee, H.J. Cell-penetrating peptide-functionalized quantum dots for intracellular delivery. *J. Nanosci. Nanotechnol.*, **2010**, *10*(12), 7897-7905.
- Liu, B.R.; Huang, Y.W.; Chiang, H.J.; Lee, H.J. Primary effectors in the mechanisms of transmembrane delivery of arginine-rich cell-penetrating peptides. *Adv. Stud. Biol.*, **2013**, *5*, 11-25.
- Lu, S.W.; Hu, J.W.; Liu, B.R.; Lee, C.Y.; Li, J.F.; Chou, J.C.; Lee, H.J. Arginine-rich intracellular delivery peptides synchronously deliver covalently and noncovalently linked proteins into plant cells. *J. Agric. Food Chem.*, **2010**, *58*(4), 2288-2294.
- Wadia, J.S.; Dowdy, S.F. Protein transduction technology. *Curr. Opin. Biotechnol.*, **2002**, *13*(1), 52-56.
- Chen, Y.J.; Liu, B.R.; Dai, Y.H.; Lee, C.Y.; Chan, M.H.; Chen, H.H.; Chiang, H.J.; Lee, H.J. A gene delivery system for insect cells mediated by arginine-rich cell-penetrating peptides. *Gene*, **2012**, *493*(2), 201-210.
- Dai, Y.H.; Liu, B.R.; Chiang, H.J.; Lee, H.J. Gene transport and expression by arginine-rich cell-penetrating peptides in Paramecium. *Gene*, **2011**, *489*(2), 89-97.
- Hou, Y.W.; Chan, M.H.; Hsu, H.R.; Liu, B.R.; Chen, C.P.; Chen, H.H. Transdermal delivery of proteins mediated by non-covalently associated arginine-rich intracellular delivery peptides. *Exp. Dermatol.*, **2007**, *16*(12), 999-1006.
- Liu, B.R.; Chiang, H.J.; Huang, Y.W.; Chan, M.H.; Chen, H.H.; Lee, H.J. Cellular internalization of quantum dots mediated by cell-penetrating peptides. *Pharm. Nanotech.*, **2013**, *1*, 151-61.
- Liu, B.R.; Huang, Y.W.; Aronstam, R.S.; Lee, H.J. Comparative mechanisms of protein transduction mediated by cell-penetrating peptides in prokaryotes. *J. Membr. Biol.*, **2015**, *248*(2), 355-368.
- Liu, B.R.; Lin, M.D.; Chiang, H.J.; Lee, H.J. Arginine-rich cell-penetrating peptides deliver gene into living human cells. *Gene*, **2012**, *505*(1), 37-45.
- Liu, B.R.; Liou, J.S.; Chen, Y.J.; Huang, Y.W.; Lee, H.J. Delivery of nucleic acids, proteins, and nanoparticles by arginine-rich cell-penetrating peptides in rotifers. *Mar. Biotechnol. (NY)*, **2013**, *15*(5), 584-595.
- Karagiannis, E.D.; Urbanska, A.M.; Sahay, G.; Pelet, J.M.; Jhunjhunwala, S.; Langer, R.; Anderson, D.G. Rational design of a biomimetic cell penetrating peptide library. *ACS Nano.*, **2013**, *7*(10), 8616-8626.
- Bellamy, W.; Takase, M.; Yamauchi, K.; Wakabayashi, H.; Kawase, K.; Tomita, M. Identification of the bactericidal domain of lactoferrin. *Biochim. Biophys. Acta.*, **1992**, *1121*(1-2), 130-136.
- Zhang, Y.; Lima, C.F.; Rodrigues, L.R. Anticancer effects of lactoferrin: Underlying mechanisms and future trends in cancer therapy. *Nutr. Rev.*, **2014**, *72*(12), 763-773.
- Yin, C.; Wong, J.H.; Ng, T.B. Recent studies on the antimicrobial peptides lactoferricin and lactoferrampin. *Curr. Mol. Med.*, **2014**, *14*(9), 1139-1154.
- Fang, B.; Guo, H.Y.; Zhang, M.; Jiang, L.; Ren, F.Z. The six amino acid antimicrobial peptide bLfcin6 penetrates cells and delivers siRNA. *FEBS J.*, **2013**, *280*(4), 1007-1017.
- Liu, B.R.; Huang, Y.W.; Aronstam, R.S.; Lee, H.J. Identification of a short cell-penetrating peptide from bovine lactoferricin for intra-

- cellular delivery of DNA in human A549 Cells. *PLoS One*, **2016**, *11*(3), e0150439.
- [34] Shin, M.C.; Zhang, J.; Min, K.A.; Lee, K.; Byun, Y.; David, A.E.; He, H.; Yang, V.C. Cell-penetrating peptides: Achievements and challenges in application for cancer treatment. *J. Biomed. Mater. Res. A.*, **2014**, *102*(2), 575-587.
- [35] Liu, B.R.; Huang, Y.W.; Winiarz, J.G.; Chiang, H.J.; Lee, H.J. Intracellular delivery of quantum dots mediated by a histidine- and arginine-rich HR9 cell-penetrating peptide through the direct membrane translocation mechanism. *Biomaterials*, **2011**, *32*(13), 3520-3537.
- [36] Liu, B.R.; Li, J.F.; Lu, S.W.; Leel, H.J.; Huang, Y.W.; Shannon, K.B.; Aronstam, R.S. Cellular internalization of quantum dots non-covalently conjugated with arginine-rich cell-penetrating peptides. *J. Nanosci. Nanotechnol.*, **2010**, *10*(10), 6534-6543.
- [37] He, Z.; Proudfoot, C.; Whitelaw, C.B.; Lillico, S.G. Comparison of CRISPR/Cas9 and TALENs on editing an integrated EGFP gene in the genome of HEK293FT cells. *SpringerPlus*, **2016**, *5*(1), 814.
- [38] Newman, A.C.; Scholefield, C.L.; Kemp, A.J.; Newman, M.; McIver, E.G.; Kamal, A.; Wilkinson, S. TBK1 kinase addition in lung cancer cells is mediated via autophagy of Tax1bp1/Ndp52 and non-canonical NF-kappaB signalling. *PLoS One*, **2012**, *7*(11), e50672.
- [39] Krasny, L.; Paul, A.; Wai, P.; Howard, B.A.; Natrajan, R.C.; Huang, P.H. Comparative proteomic assessment of matrixome enrichment methodologies. *Biochem. J.*, **2016**, *473*(21), 3979-3995.
- [40] Colin, F.C.; Schrier, S.L. Spontaneous endocytosis in human neonatal and adult red blood cells: comparison to drug-induced endocytosis and to receptor-mediated endocytosis. *Am. J. Hematol.*, **1991**, *37*(1), 34-40.
- [41] Wang, M.; Zhang, Y.; Feng, J.; Gu, T.; Dong, Q.; Yang, X.; Sun, Y.; Wu, Y.; Chen, Y.; Kong, W. Preparation, characterization, and *in vitro* and *in vivo* investigation of chitosan-coated poly (d,l-lactide-co-glycolide) nanoparticles for intestinal delivery of endostatin. *Int. J. Nanomed.*, **2013**, *8*, 1141-1154.
- [42] Liu, B.R.; Lo, S.Y.; Liu, C.C.; Chyan, C.L.; Huang, Y.W.; Aronstam, R.S.; Lee H.J. Endocytic trafficking of nanoparticles delivered by cell-penetrating peptides comprised of nona-arginine and a penetration accelerating sequence. *PLoS One*, **2013**, *8*(6), e67100.
- [43] Brock, R. The uptake of arginine-rich cell-penetrating peptides: Putting the puzzle together. *Bioconjug. Chem.*, **2014**, *25*(5), 863-868.
- [44] Ramsey, J.D.; Flynn, N.H. Cell-penetrating peptides transport therapeutics into cells. *Pharmacol. Ther.*, **2015**, *154*, 78-86.
- [45] Liu, B.R.; Liou, J.S.; Huang, Y.W.; Aronstam, R.S.; Lee, H.J. Intracellular delivery of nanoparticles and DNAs by IR9 cell-penetrating peptides. *PLoS One*, **2013**, *8*(5), e64205.
- [46] Harreither, E.; Rydberg, H.A.; Amand, H.L.; Jadhav, V.; Fliedl, L.; Benda, C.; Esteban, M.A.; Pei, D.; Borth, N.; Grillari-Voglauer, R.; Hommerding, O.; Edenhofer, F.; Nordén, B.; Grillari, J. Characterization of a novel cell penetrating peptide derived from human Oct4. *Cell Regen. (Lond.)*, **2014**, *3*(1), 2.
- [47] Hughes, S.R.; Dowd, P.F.; Johnson, E.T. Cell-penetrating recombinant peptides for potential use in agricultural pest control applications. *Pharmaceuticals (Basel)*, **2012**, *5*(10), 1054-1063.
- [48] Liu, B.R.; Chen, H.H.; Chan, M.H.; Huang, Y.W.; Aronstam, R.S.; Lee, H.J. Three arginine-rich cell-penetrating peptides facilitate cellular internalization of red-emitting quantum dots. *J. Nanosci. Nanotechnol.*, **2015**, *15*(3), 2067-2078.
- [49] Hwang, P.M.; Zhou, N.; Shan, X.; Arrowsmith, C.H.; Vogel, H.J. Three-dimensional solution structure of lactoferricin B, an antimicrobial peptide derived from bovine lactoferrin. *Biochemistry*, **1998**, *37*(12), 4288-4298.
- [50] Farnaud, S.; Patel, A.; Odell, E.W.; Evans, R.W. Variation in antimicrobial activity of lactoferricin-derived peptides explained by structure modelling. *FEMS Microbiol. Lett.*, **2004**, *238*(1), 221-226.
- [51] Hilchie, A.L.; Vale, R.; Zemlak, T.S.; Hoskin, D.W. Generation of a hematologic malignancy-selective membranolytic peptide from the antimicrobial core (RRWQWR) of bovine lactoferricin. *Exp. Mol. Pathol.*, **2013**, *95*(2), 192-198.
- [52] Manceur, A.P.; Audet, J. Measurement of cell-penetrating peptide-mediated transduction of adult hematopoietic stem cells. *Methods Mol. Biol.*, **2009**, *482*, 43-54.